Supporting Information:

Aggregation-induced emission leading to two distinct emissive species in the solid-state structure of high-dipole organic chromophores

Felix Witte,[1]* Philipp Rietsch,[2] Nithiya Nirmalananthan-Budau,[3] Florian Weigert,[3]
Jan P. Götze,[1] Ute Resch-Genger,[3] Siegfried Eigler,[2] and Beate Paulus[1]

[1] Dr. F. Witte, Dr. J. P. Götze, Prof. Dr. B. Paulus
Institute of Chemistry and Biochemistry
Freie Universität Berlin
Arnimallee 22, 14195 Berlin, Germany
E-mail: jf.witte@fu-berlin.de

[2] Dr. P. Rietsch, Prof. Dr. S. Eigler
Institute of Chemistry and Biochemistry
Freie Universität Berlin
Takustr. 3, 14195 Berlin, Germany

[3] Dr. N. Nirmalananthan-Budau, F. Weigert, Dr. U. Resch-Genger
Division Biophotonics
Federal Institute for Material Research and Testing (BAM)
Richard-Willstätter-Straße 11, 12489 Berlin, Germany

Contents

1 General information

All reagents were purchased from commercial sources and used without further purification. Dry solvents were purchased from Acros Organics. ALUGRAM Xtra SIL G/UV^{254} plates by Macherey-Nagel were used for thin-layer chromatography. Isolation of products by chromatography was performed with silica from Macherey-Nagel Silica 60 M (0.04–0.063 mm). NMR spectra were recorded on a JOEL ECX 400 (^{1}H 400 MHz, ^{13}C 101 MHz), JEOL Eclipse+ 500 (^{1}H 500 MHz, ^{13}C 126 MHz) and BRUKER AVANCE 700 (1H 700 MHz, 13C 176 MHz) spectrometer at 25 °C. The chemical shifts δ are calibrated on the respective solvent peak as internal standard. All shifts are reported in ppm and NMR multiplicities are abbreviated as s (singlet), d (duplet), t (triplet), m (multiplet). Coupling constants J are reported in Hz. UV/Vis spectra were recorded on a Cary 50 Bio photospectrometer (Varian). Fluorescence spectra were recorded on a LS 50 B luminescence spectrometer from PerkinElmer. UV/Vis and Fluorescence spectra were measured in quartz glass cuvettes with 1 cm path length. IR Spectra were recorded on a FT/IR 4100 spectrometer from JASCO. Elemental analysis was performed on an VARIO EL from Elementar. Photoluminescence quantum yields (Φ_{fl}) were determined absolutely with an integrating sphere setup from Hamamatsu (Quantaurus-QY C11347-11). All Φ_{fl} measurements were performed at 25 °C using special 10 mm x 10 mm long neck quartz cuvettes from Hamamatsu. Values below 1% quantum yield are not reliable in the measurement setup and are therefore given as < 1%.

The fluorescence lifetime (τ), the average time in which the fluorophore is in an excited state before it relaxes to the ground state, was recorded on a fluorometer FLS 920 (Edinburgh Instruments) equipped with a Hamamatsu R3809U-50 (range 200–850 nm, response width <25 ps), Multi-Channel Plate (MCP) detector, Czerny-Turner double monochromators and either a supercontinuum laser (Fianium SC400-2-PP) or a Edinburgh Instrument EPLED-330 (picosecond pulsed light emitting diode) for excitation at 375 nm, or a Edinburgh Instrument EPL-375 (picosecond pulsed diode laser) for excitation at 330 nm. All the measurements were performed at T = 298 K using 10 mm–10 mm quartz cuvettes from Hellma GmbH always filled with 2 mL of solvent or dye solution. Before each measurement, the instrument response function (IRF) was measured. The lifetime measurements were analysed with Edinburgh Instruments FAST Software and fitted with a reconvolution fit. All the lifetimes could be evaluated mono, bi- or tri-exponentially with a reduced χ^2 between 0.8 and 3.0.

The fluorescence spectra of the crystals in the solid-state and microscopic images were recorded with an Olympus FluoView FV1000 (Olympus GmbH, Hamburg, Germany). For UV excitation, a DPSS Cobolt Zouk® (355 nm; 10 mW), and for transmission imaging an additional multiline argon ion laser (30 mW, 488 nm) were used as excitation sources, which were reflected by a beamsplitter (BS 20/80) and focused onto the sample through an Olympus objective UPLSAPO 10X (numerical aperture N.A. 0.40). The emitted photons were recollected with the same objective and focused onto a PMT. Emission signals were detected in a wavelength range between 460 nm and 700 nm with spectral resolution of 5 nm and a step width of 2 nm. The spatial resolved fluorescence spectra are raw spectra, not specifically corrected for the wavelength-dependent spectral responsivity of the detection system of the microscope.

Single crystal measurements were performed using an inverted confocal microscope setup with an oil immersion 100x objective. The samples were prepared by dispersing a low amount of crystals onto a fresh glass coverslip. Sample emission was recorded under pulsed excitation at 405 nm and a repetition rate of 10 MHz. Detection of stray excitation light was suppressed by using a dichroic long pass mirror. The spectral range from which emission was detected was selected by using different long and short pass filters with the PL signal being either recorded with an EM-CCD or a SPAD single-photon-sensitive detector with time correlated single photon counting capability in order to obtain spectra or decay kinetics, respectively.

2 Synthetic procedures and spectral characterization

The synthesis of **1**, **2** and **4** was done according to literature.[1] For compound **3** the diamine **5** was synthesized as shown in **Fig. S1** and described in detail below via the imine intermediate which was not isolated. The numbers of the compounds were chosen for an easier understanding in the paper. The NMR spectra of **1–4** are given at the end of this document.
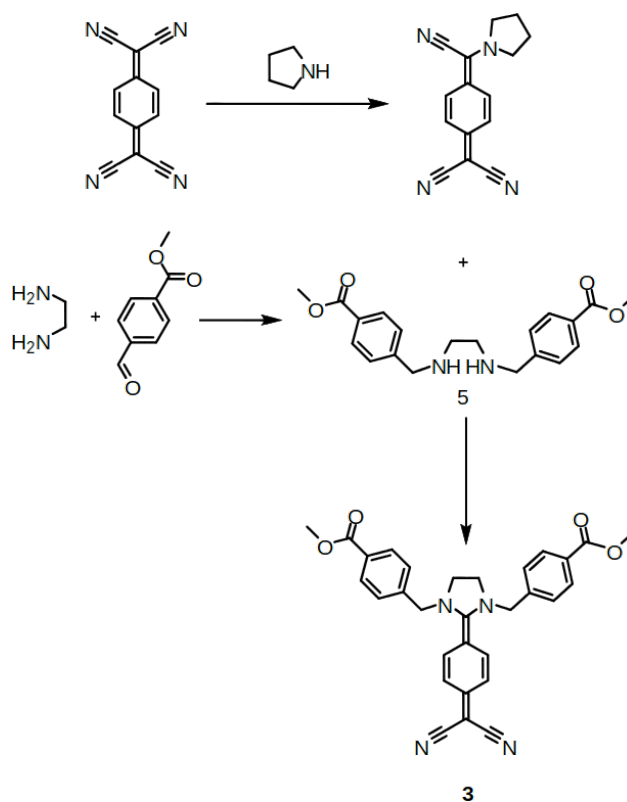
Figure S1: Synthetic route towards diaminodicyanoquinone derivative **3**.

2.1 2-(4-(1,3-dineopentylimidazolidin-2-ylidene)cyclohexa-2,5-dien-1-ylidene) malononitrile (1)
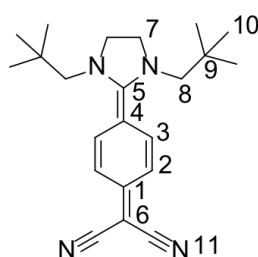
N,N'-dineopentylethane-1,2-diamine (95 mg, 0.47 mmol, 1 eq.), dissolved in acetonitrile (5 mL), was added to a 40 °C warm solution of compound **6** (117.7 mg, 0.47 mmol, 1 eq.) in acetonitrile (7 mL). After 4 hours at 75 °C the solution was deep yellow and allowed to cool to room temperature over night. The precipitate, a yellow powder, was filtered off, washed with cooled acetonitrile (3x 3 mL) and recrystallized in acetonitrile to form neat orange crystals (113.9 mg, 0.32 mmol, 65.4%).

1H NMR (500 MHz, DMSO-d_6, RT): δ (ppm) = 7.11 (d, 2H, ^3J = 10.0 Hz, 2), 6.86 (d, 2H, ^3J = 10.0 Hz, 3), 4.03 (s, 4H, 7), 3.11 (s, 4H, 8), 0.78 (s, 18H, 10)

13C NMR (125 MHz, DMSO-d_6, RT): δ (ppm) = 168.87 (1C, 6), 146.96 (1C, 5), 129.73 (1C, 1), 124.57 (2C, 2), 118.08 (2C, 3), 109.05 (2C, 11), 87.58 1C, 4), 58.77 (2C, 8), 50.86 (2C, 7), 33.10 (2C, 9), 28.33 (6C, 10)

FT-IR (ATR) $\tilde{\nu}$ (cm^{-1}): 2975 (s), 2891 (m), 1648 (m), 1455 (w), 1418 (m), 1378 (m), 1318 (vw), 1085 (vs), 1045 (s), 879 (s)

UV/Vis (Ethanol) λ_{max} nm (ε [Lmol^{-1} cm^{-1}]): 363 (16218)

UV/Vis (Methanol) λ_{max} nm (ε [Lmol^{-1} cm^{-1}]): 354 (16800)

UV/Vis (THF) λ_{max} nm (ε [Lmol^{-1} cm^{-1}]): 334 (6250), 410 (22750)

4

UV/Vis (ACN) λ_{max} nm (ε [Lmol^{-1} cm^{-1}]): 362 (11500)
UV/Vis (DMSO) λ_{max} nm (ε [Lmol^{-1} cm^{-1}]):
UV/Vis (DMF) λ_{max} nm (ε [Lmol^{-1} cm^{-1}]): 366 (12000)
MS (EI): m/z = 389.21 (10) [M-K$^+$]; 373.24 (25) [M-Na$^+$]; 351.25 (100) [M$^+$] 281.18 (8), 211.10 (5)
EA: C$_{22}$H$_{30}$N$_4$; calc.: C, 75.39; N, 15.98; H, 8.63 meas.: C, 75.39; N, 16.04; H, 8.77

2.2 2-(4-(1,3-Dimethylimidazolidin-2-yliden)cyclohexa-2,5-dien-1-yliden)malononitrile (2)

N,N'-Dimethylethylendiamin (71 mg, 0.087 mL, 0.81 mmol, 1 eq.) was added to a 40 °C warm solution of compound **6** (2-(4-(cyano(pyrrolidin-1-yl)methylene)cyclohexa-2,5-dien-1-ylidene)malononitrile) (200 mg, 0.81 mmol, 1 eq.) in 25 mL acetonitrile. The solution was stirred at 70 °C for 4 hours and then cooled to room temperature. The precipitate was filtered off and washed with cooled acetonitrile (3x 10 mL) to yield the product as a yellow powder (75.7 mg, 0.32 mmol, 39%).

^{1}H NMR (700 MHz, DMSO-d$_6$, RT): δ (ppm) = 7.19 (d, ^{3}J = 8.7 Hz, 2H, 4), 6.89 (d, ^{3}J = 8.7 Hz, 2H, 5), 3.90 (s, 4H, 8), 2.96 (s, 6H, 9).
^{13}C NMR (125 MHz, DMSO-d$_6$, RT): δ (ppm) = 166.35 (1C, 2), 148.35 (1C, 7), 130.01 (1C, 3), 124.03 (2C, 4), 118.03 (2C, 5), 107.79 (1C, 1), 50.21 (1C, 6), 35.45 (2C, 8), 32.95 (2C, 9).
FT-IR (ATR) $\tilde{\nu}$ (cm^{-1}): 2932 (w), 2171 (s), 2132 (s), 1595 (s), 1499 (m), 1370 (m), 1324 (m), 1297 (m), 936 (m), 827 (s)
UV/Vis (ACN) λ_{max} nm (ε [Lmol^{-1} cm^{-1}]): 377 (22800).
UV/Vis (DMF) λ_{max} nm (ε [Lmol^{-1} cm^{-1}]): 385 (25000).
UV/Vis (DMSO) λ_{max} nm (ε [Lmol^{-1} cm^{-1}]): 381 (23500).
UV/Vis (MeOH) λ_{max} nm (ε [Lmol^{-1} cm^{-1}]): 368 (23900).
UV/Vis (THF) λ_{max} nm (ε [Lmol^{-1} cm^{-1}]): 416 (4300).
MS (EI): m/z = 239.12 (100) [MH]$^+$; 238.12 (27) [M]$^{\cdot+}$, 180.98 (58), 166.02 (25), 68.99 (30).
EA: C$_{13}$H$_{12}$N$_4$; calc.: C, 70.57; N, 23.51; H, 5.92; meas.: C, 68.22; N, 25.76; H, 5.03.

2.3 Dimethyl 4,4'-((2-(4-(dicyanomethylene)cyclohexa-2,5-dien-1-ylidene)imidazolidine-1,3-diyl)bis(methylene))dibenzoate (3)
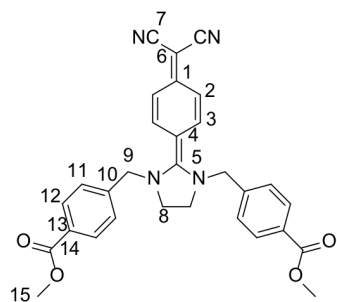
Under argon atmosphere, Dimethyl 4,4'-((ethane-1,2-diylbis(azanediyl))bis-(methylene))dibenzoate (300.00 mg, 1.21 mmol), dissolved in acetonitrile (15 mL), was added to a 40 °C warm solution of Compound **6** (430.65 mg; 1.21 mmol) in acetonitrile (20 mL). The solution turned yellow after 20 hours at 70 °C. After cooling to room temperature, the solution stood for 1 day in the fridge. Filtration then yielded fine yellow crystal needles which were washed with cooled acetonitrile (3x 5 mL) to yield compound **3** (403.86 mg; 0.79 mmol; 66.0%).

^{1}H NMR (500 MHz, DMSO-d$_6$, RT): δ (ppm) = 8.00 (d, ^{3}J = 8.5 Hz, 4H, 12), 7.50 (d, ^{3}J = 8.5 Hz, 4H, 11), 7.19 (d, ^{3}J = 9.0 Hz, 2H, 3), 6.84 (d, ^{3}J = 9.0 Hz, 2H, 2), 4.64 (t, ^{3}J = 20.0 Hz, 4H, 8), 3.88 (s, 4H, 9), 3.87 (s, 6H, 15)
^{13}C NMR (176 MHz, DMSO-d$_6$, RT): δ (ppm) = 169.19 (1C, 5), 166.48 (2C, 14), 148.78 (1C, 4), 141.37 (2C, 13), 140.55 (1C, 6); 130.30 (4C, 12), 129.89 (2C, 10), 129.36 (2C, 3), 128.40 (4C, 11), 118.51 (2C, 2), 107.75 (2C, 7), 51.83 (2C, 8), 52.85 (2C, 15), 48.58 (2C, 9)
FT-IR (ATR) $\tilde{\nu}$ (cm^{-1}): 3025 (vw), 2945 (w), 2841 (vw), 2361 (w), 2171 (s), 2129 (s), 1719 (s), 1596 (m), 1555 (s), 1491 (m), 1432 (m), 1375 (w), 1320 (m), 1267 (s), 1188 (m), 1107 (m), 1014 (m), 920 (m), 844 (m), 820 (m), 747 (m)
UV/Vis (Ethanol) λ_{max} nm (ε [Lmol^{-1} cm^{-1}]): 234 (4.35), 393 (4.24)

MS (EI): m/z = 1542.57 $[HNa-M_3]^+$ (8), 1035.38 $[HNa-M_2]^+$ (50), 529.18 $[HNa-M_2]^+$ (100), 507.20 $[H-M]^+$ (20)

EA: $C_{30}H_{26}N_4O_4$; calc.: C, 71.13; N, 11.06; H, 5.17 meas.: C, 70.83; N, 11.28; H, 5.27

2.4 2-(4-(1,3-dihydro-2H-benzo[d]imidazol-2-ylidene)cyclohexa-2,5-dien-1-ylidene) malononitrile (4)
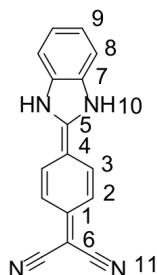
Under argon atmosphere, ortho-Phenylendiamine (70.0 mg, 0.64 mmol, 1 eq.), dissolved in acetonitrile (15 mL), was added to a 40 °C warm solution of Compound **6** (160.0 mg, 0.64 mmol, 1 eq.) in acetonitrile (20 mL). The solution turned red after 20 hours at 70 °C. After cooling to room temperature, the solution stood for 4 days in the fridge. Filtration then yielded a fine grain greenish powder which was washed with cooled acetonitrile (3x 5 mL). The product was recrystallized from acetonitrile to yield fine yellow crystals (70.2 mg, 0.27 mmol, 42.5%).

^{1}H NMR (700 MHz, DMSO-d_6, RT): δ (ppm) = 14.35 (bs, 2H, 10), 7.86 (d, ^3J = 8.7 Hz, 2H, 2), 7.69 (q, ^3J = 8.7 Hz, 2H, 9), 7.47 (q, ^3J = 8.6 Hz, 2H, 8), 6.95 (d, ^3J = 8.7 Hz, 2H, 3)

^{13}C NMR (176 MHz, DMSO-d_6, RT): δ (ppm) = 150.27 (1C, 6), 149.31 (1C, 5), 132.26 (1C, 1), 128.54, 126.54 (1C, 2), 125.48 (2C, 8), 123.51 (2C, 7), 118.49 (2C, 3), 113.47 (2C, 9), 79.63 (1C, 4)

FT-IR (ATR) $\tilde{\nu}$ (cm^{-1}): 2952 (w), 2877 (w), 2849 (w), 2761 (w), 2190 (s), 2140 (s), 1637 (w), 1612 (m), 1503 (m), 1459 (m), 1387 (m), 1336 (m), 1230 (m), 1201 (m), 819 (s), 742 (s)

UV/Vis (DMF) λ_{max} nm (ε [Lmol^{-1} cm^{-1}]): 391 (56500)

UV/Vis (ACN) λ_{max} nm (ε [Lmol^{-1} cm^{-1}]): 385 (86800)

UV/Vis (DMSO) λ_{max} nm (ε [Lmol^{-1} cm^{-1}]): 392 (42200)

UV/Vis (THF) λ_{max} nm (ε [Lmol^{-1} cm^{-1}]): 388 (7000)

UV/Vis (MeOH) λ_{max} nm (ε [Lmol^{-1} cm^{-1}]): 424 (20000)

MS (EI): m/z = 259.10 (15), 258.09 $[MH]^{\cdot+}$ (100), 257.10 (5), 232 (5).

EA: $C_{16}H_{16}N_4$; calc.: C, 74.40; N, 21.69; H, 3.90; meas.: C, 74.31; N, 21.78; H, 4.07

2.5 Dimethyl 4,4'-((ethane-1,2-diylbis(azanediyl))bis(methylene))dibenzoate (5)
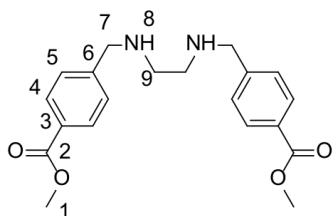
Ethane-1,2-diamine (1 g, 16.64 mmol) was added dropwise with stirring to a solution of methyl 4-formylbenzoate (6.28 g, 38.27 mmol) in 30 mL of dry methanol. The mixture was stirred for 4 days. After addition of 100 ml dry methanol, NaBH$_4$ (3.15 g; 83.19 mmol) was added and the mixture was stirred ON. Cooling in ice water precipitated a white solid which was filtered off and washed with cooled H$_2$O (2x 50 mL), ethanol (2x 25 mL), and dried under vacuum.

^{1}H NMR (500 MHz, DMSO-d_6, RT): δ (ppm) = 7.90 (d, ^3J = 6.0 Hz, 4H, 4), 7.46 (d, ^3J = 6.0 Hz, 4H, 5), 3.80 (s, 6H, 1), 3.70 (s, 4H, 7), 2.58 (s, 4H, 9), 2.25 (bs, 2H, 8)

^{13}C NMR (176 MHz, DMSO-d_6, RT): δ (ppm) = 166.79 (2C, 2), 147.62 (4C, 3), 129.59 (4C, 4), 128.58 (2C, 5), 128.40 (2C, 3), 53.11 (2C, 9), 52.56 (2C, 1), 48.98 (2C, 7)

MS (EI): m/z = 379.16 $[Na-M]^+$ (25), 357.18 $[MH]^{\cdot+}$ (100), 326.37 (15), 192.10 (15), 149.06 (10)

2.6 2-(4-(cyano(pyrrolidin-1-yl)methylene)cyclohexa-2,5-dien-1-ylidene)malononitrile (6)
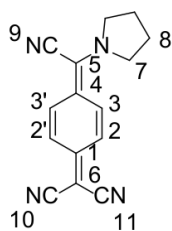
To a stirred warm solution of TCNQ (250.0 mg, 1.22 mmol, 1 eq.) in acetonitrile (20 mL), pyrrolidine (69.7 mg, 0.98 mmol, 0.8 eq.) was added in one shot. The solution turned green and then purple. After stirring for 4 hours at 70 °C the solution was cooled to room temperature and then stored in the fridge for 3 days. The precipitate was filtered and washed with cooled acetonitrile (3x 5 mL) to yield the product as fine purple crystal needles (232.4 mg, 0.93 mmol, 76.5%).

^{1}H NMR (400 MHz, DMSO-d_6, RT): δ (ppm) = 7.73 (dt, ^4J = 0.7Hz, ^3J = 7Hz, 2H, 3), 7.81 (dt, ^4J = 0.7Hz, ^3J = 7Hz, 2H, 2), 4.11 (bs, 4H, 7), 2.08 (m, 4H, 8)

^{13}C NMR (100 MHz, DMSO-d_6, RT): δ (ppm) = 153.95 (1C, 6), 137.76 (1C, 4), 134.32 (2C, 2), 120.11 (2C, 3), 118.92 (1C, 10), 116.78 (1C, 11), 113.09 (1C, 9), 57.40(1C, 6), 50.92 (2C, 7), 25.60 (2C, 8)

FT-IR (ATR) $\tilde{\nu}$ (cm^{-1}): 2190 (m), 2164 (s), 1611 (s), 1536 (m), 1474 (w), 1381 (s), 1341 (m), 1207, (s), 861 (s), 823 (s), 727 (m), 650 (s)

UV/Vis (ACN) λ_{max} nm (ε [Lmol^{-1} cm^{-1}]): 275 (6300), 480 (13000)

MS (EI): m/z = 249.1 (20); 248.0 (100)[MH]$^{\cdot+}$; 221.1 (15); 179.1 (17); 154.1 (20)

EA: $C_{15}H_{12}N_4$; calc.: C, 72.56; H, 4.87; N, 22.57, meas.: C, 72.74; N, 21.57; H, 4.89

3 Crystal structures

3.1 Data

Table S1: Crystal data and structure refinement for **1**. Compound **1** has already been published in ref.[1]

Identification code	NN_Neopentyl_Ethan
Empirical formula	$C_{22}H_{30}N_4$
Formula weight	350.5
Temperature/K	100(2)
Crystal system	monolinic
Space group	P21/c
a/Å	9.3411(2)
b/Å	19.6042(3)
c/Å	11.8719(2)
α	90
β	109.8547(7)
γ	90
Volume/Å^3	2044.81(6)
Z	4
$\rho_{calc}g/cm^3$	1.139
μ/mm^{-1}	0.068
F(000)	760
Crystal size/mm^3	0.560 x 0.480 x 0.180
Radiation	MoKα ($\lambda = 0.71073$)
2θ range for data collection/°	4.636 to 51.464
Index ranges	$-11 \leq h \leq 11$, $-23 \leq k \leq 23$, $-14 \leq l \leq 14$
Reflections collected	19722
Independent reflections	3889 [$R_{int} = 0.0310$, $R_{sigma} = 0.0228$]
Data/restraints/parameters	3889/0/242
Goodness-of-fit on F^2	1.037
Final R indexes [I$\geq 2\sigma$ (I)]	$R_1 = 0.0384$, $wR_2 = 0.0918$
Final R indexes [all data]	$R_1 = 0.0444$, $wR_2 = 0.0954$
Largest diff. peak/hole / e Å^{-3}	0.30/-0.21

Table S2: Crystal data and structure refinement for **2**. Compound **2** has already been published in ref.[2]

Identification code	NN_Methyl_Ethan
Empirical formula	$C_{28}H_{28}N_8$
Formula weight	476.58
Temperature/K	100(2)
Crystal system	monoclinic
Space group	P21/c
a/Å	9.1324(7)
b/Å	11.5952(8)
c/Å	11.7818(7)
α	90
β	98.419(2)
γ	90
Volume/Å^3	1234.15(15)
Z	2
ρ_{calc}g/cm^3	1.282
μ/mm^{-1}	0.08
F(000)	504
Crystal size/mm^3	0.13 x 0.12 x 0.12
Radiation	MoKα ($\lambda = 0.71073$)
2θ range for data collection/$^\circ$	4.508 to 50.808
Index ranges	-11 $\leq$ h $\leq$ 11, -13 $\leq$ k $\leq$ 13, -13 $\leq$ l $\leq$ 14
Reflections collected	15361
Independent reflections	2259 [R_{int} = 0.0723, R_{sigma} = 0.0411]
Data/restraints/parameters	2259/0/165
Goodness-of-fit on F^2	1.055
Final R indexes [I$\geq$2σ (I)]	R_1 = 0.0413, wR_2 = 0.0874
Final R indexes [all data]	R_1 = 0.0660, wR_2 = 0.0988
Largest diff. peak/hole / e Å^{-3}	0.15/-0.31

Table S3: Crystal data and structure refinement for **3**

Identification code	PR111-sr-final
Empirical formula	C30H26N4O4
Formula weight	506.55
Temperature/K	100(2)
Crystal system	triclinic
Space group	P-1
a/Å	9.45250(10)
b/Å	11.1197(2)
c/Å	14.54330(10)
α	97.639(4)
β	108.409(4)
γ	106.008(3)
Volume/Å^3	1352.99(5)
Z	2
ρ_{calc}g/cm^3	1.243
μ/mm^{-1}	0.683
F(000)	532
Crystal	size/mm3
Radiation	CuKα ($\lambda = 1.54178$)
2θ range for data collection/$^\circ$	6.6 to 133.5
Index ranges	-9 $\leq$ h $\leq$ 11, -13 $\leq$ k $\leq$ 13, -17 $\leq$ l $\leq$ 17
Reflections collected	17026
Independent reflections	4780 [R$_{int}$ = 0.0662, R$_{sigma}$ = 0.0558]
Data/restraints/parameter s	4780/0/345
Goodness-of-fit on F^2	
Final R indexes [I$\geq$2σ (I)]	R$_1$ = 0.0495, wR$_2$ = 0.1144
Final R indexes [all data]	R$_1$ = 0.0678, wR$_2$ = 0.1237
Largest diff. peak/hole / e Å^{-3}	0.17/-0.26

Table S4: R-factors of crystal structures

	1	**2**	**3**
R-factor	3.84	4.13	4.95

3.2 Unit cells

a = 9.3411(2)
b = 19.6042(3)
c = 11.8719(2)
α = 90
β = 109.8547(7)
γ = 90

a = 9.1324(7)
b = 11.5952(8)
c = 11.7818(7)
α = 90
β = 98.419(2)
γ = 90

a = 9.45250(10)
b = 11.1197(2)
c = 14.54330(10)
α = 97.639(4)
β = 108.409(4)
γ = 106.008(3)
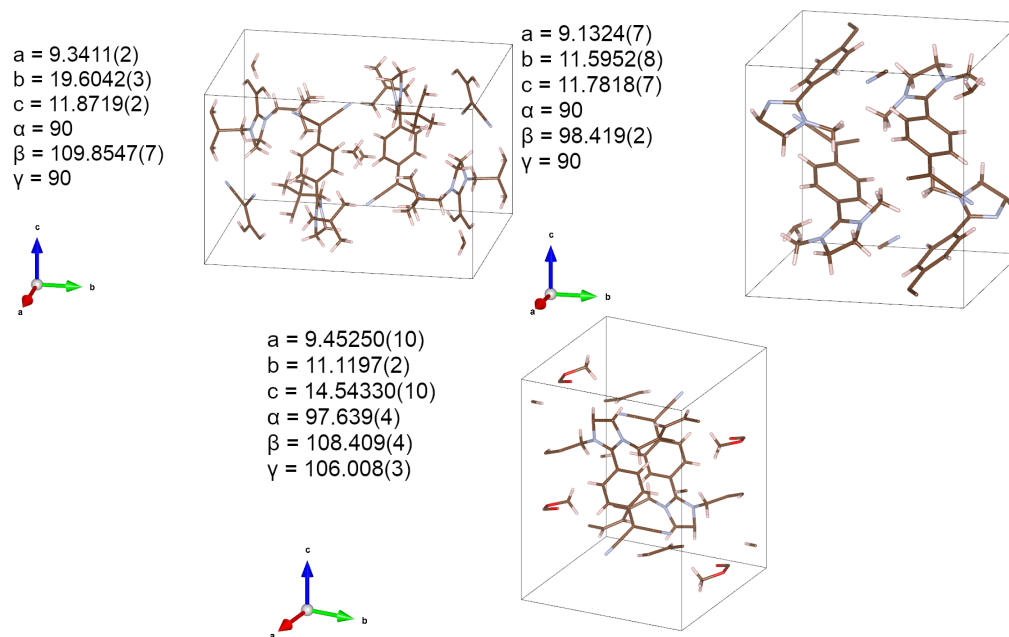
Figure S2: Unit cell with parameters of compound **1** (top left), **2** (top right), and **3** (bottom).

4   Single crystal measurements

Table S5: Average intensity weighted lifetimes τ (3-exponentail fit) of the measured decay curves of three to five single crystals of compounds **1**-**4** in different spectral windows λ_{em} (blue edge, red edge and full range) from spectrally filtered time-resolved fluorescence measurements using time-correlated single photon counting detection, σ: standard deviation.

Sample	λ_{em}/nm	τ/ns	σ/ns
	435–475	1.98	0.83
1	525–800	5.26	0.60
	435–800	4.09	1.14
	435–475	1.76	0.16
2	525–800	5.39	0.63
	435–800	2.53	0.33
	435–475	0.81	0.10
3	525–800	8.94	1.14
	435–800	7.39	0.50
	435–475	3.67	0.31
4	525–800	4.47	0.49
	435–800	4.40	0.16

5 Emission properties
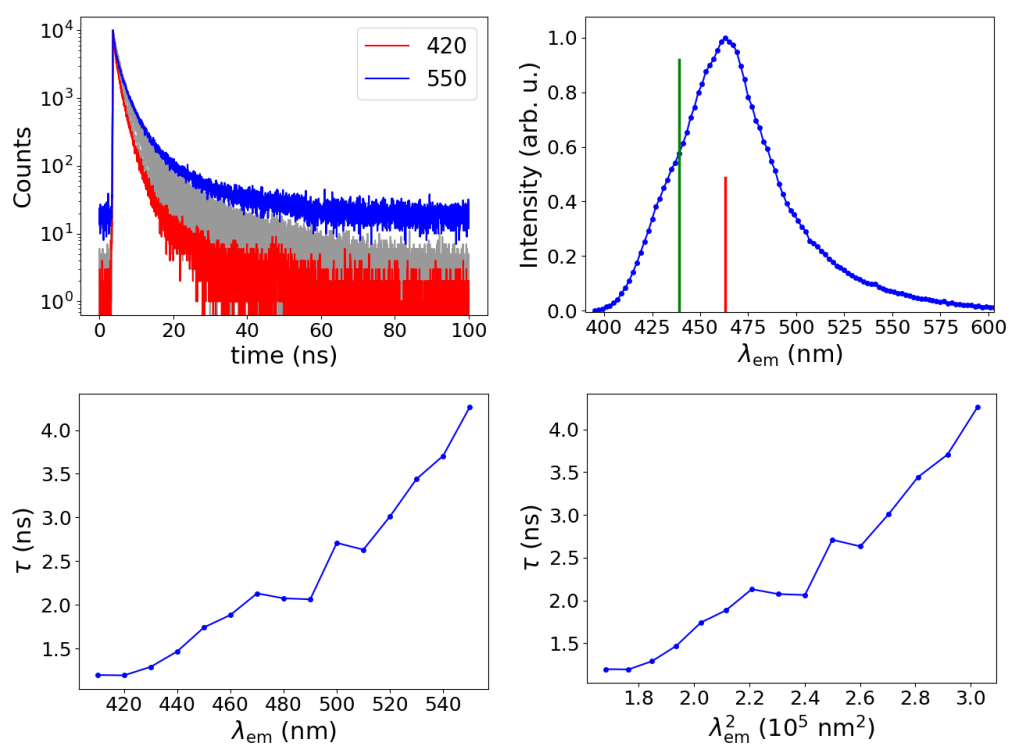
Figure S3: Emission properties of compound **2**: lifetime measurements (top left), solid-state emission spectrum with computed vertical transition lines obtained at the BHLYP/def2-SVP/MRCI level (top right), lifetime-emission wavelength dependence (bottom left), reciprocal lifetime to reciprocal squared emission wavelength dependence (bottom right).
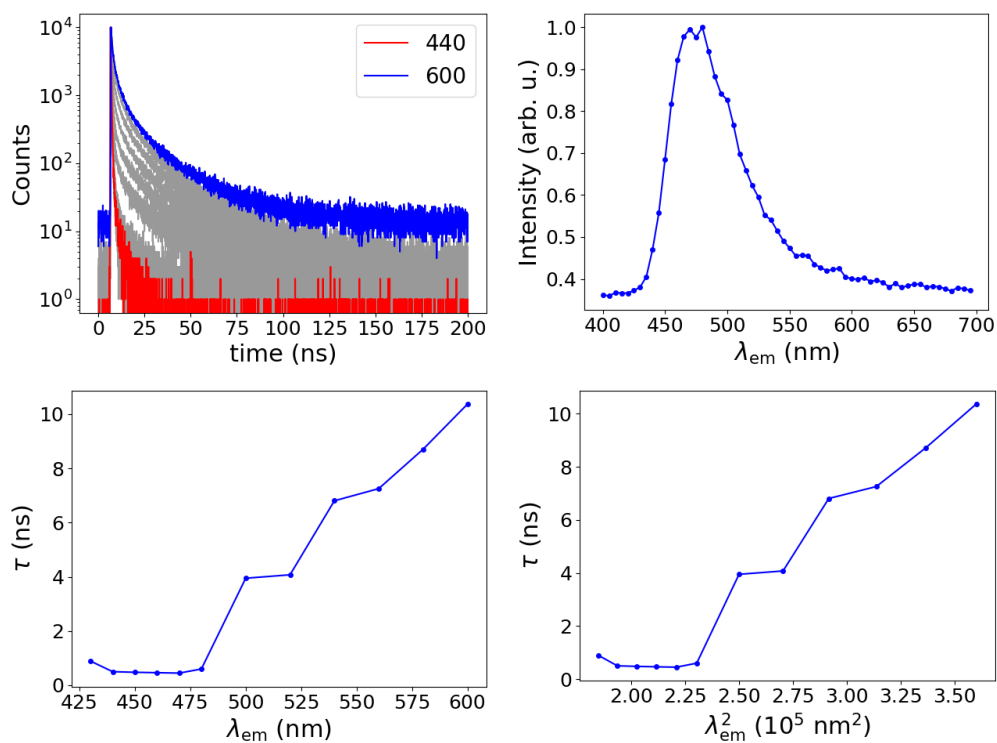
Figure S4: Emission properties of compound **3**: lifetime measurements (top left), solid-state emission spectrum (top right), lifetime-emission wavelength dependence (bottom left), reciprocal lifetime to reciprocal squared emission wavelength dependence (bottom right).
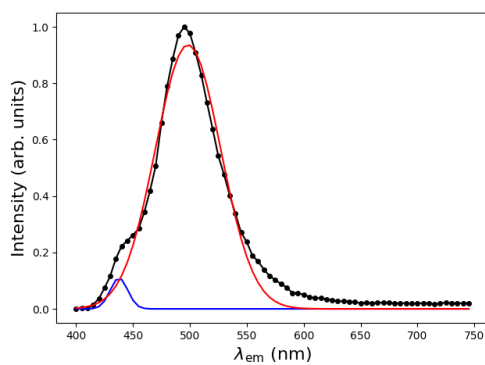
Figure S5: Gaussian fit of the emission specturm of compound **1** to estimate the emission energy of the high-energy (low-wavelength) shoulder (ca. 438 nm), ratio of the integrals: ca. 32:1 (red:blue).
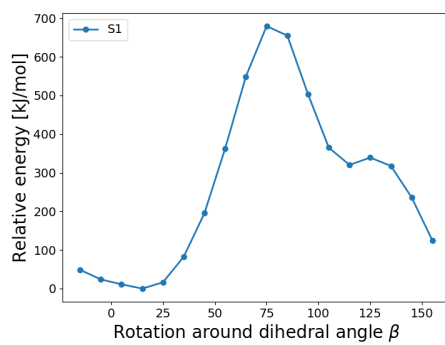
Figure S6: Lowest singlet excited state potential energy surface for the rotation of the dicyano group (dihedral angle β) of a monomer in the crystal structure of **2** estimated from an ONIOM(PBE/def2-SVP/UFF) calculation.

6 Computational Details

6.1 Förster and Dexter energy transfer rates

From the optimised solid-state structure (for optimisation procedure see below) of each compound, one molecule in the centre of a large supercell surrounded by a sphere of molecules with a radius of 10 Å was chosen to evaluate both Förster and Dexter transfer rates for each dimer that included the central structure. The total transfer rates are simply the sum of all individual contributions. As proposed Radhakrishnan and co-workers,[radhakrishnan] for Dexter rates, only neighbouring molecules of the central structure were considered for which $r\sin(\theta) < 10$ Å and $r' > 2.5$ Å (10 Å is approximately the length of one DADQ moiety, for designations, see main text). The centre of the π-plane was chosen to coincide with the centre of the benzene ring. For compound **4**, both benzene rings were regarded since the excitation is delocalised over the entire system.[1] For compound **3**, the benzene rings of the benzoate moieties were not regarded since the excited state is localised on the DADQ moiety (**Fig. S7**). **Table S6** summarises absolute values obained for k_{F} and k_{D} in comparison to solid-state QYs. **Fig. S8** illustrates the dimers that yielded the largest contribution to the transfer rates.
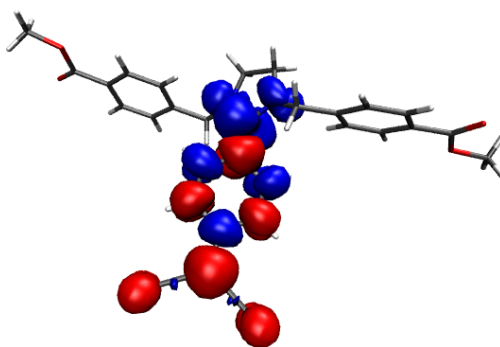
Figure S7: S_1 difference density of compound **3** obtained at the ωB97X-D3/def2-SVP[3,4] level of DFT, isovalue = 0.001 a_0^{-3}.

Table S6: Solid-state QYs and Förster and Dexter energy transfer rates of all compounds.

	solid-state QY	$k_{\mathrm{F}}/10^{-4}$	$k_{\mathrm{D}}/10^{-3}$
1	18	0.828	2.48
2	10	3.75	36.6
3	6	0.637	63.0
4	<1	9.06	210

1 **2** **3** **4**
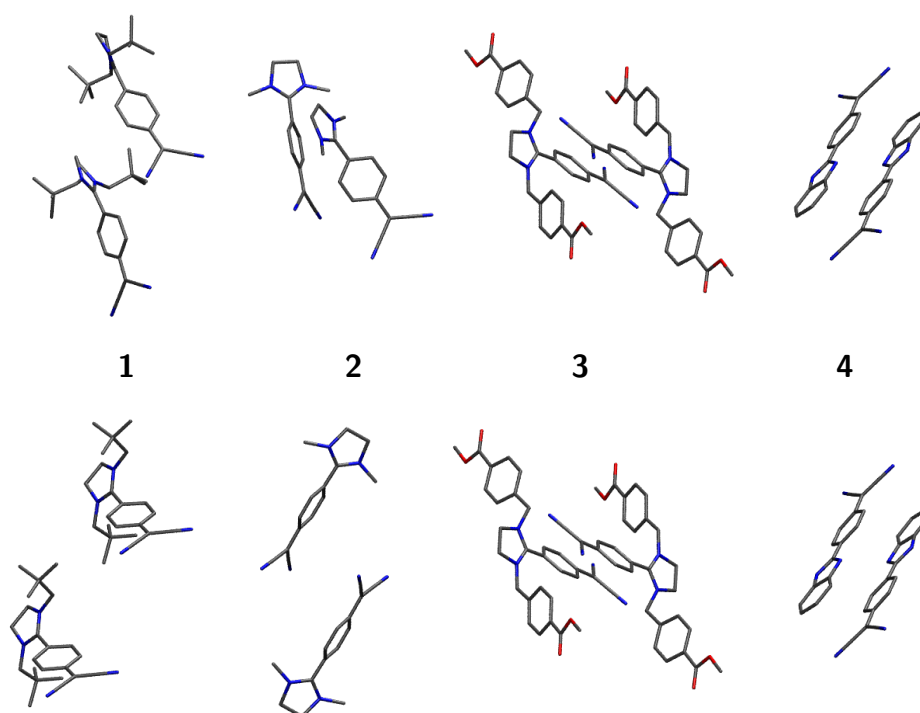
Figure S8: Structural motifs contributing most to k_{F} (top) and k_{D} (bottom) for each compound.

6.2 Calculation of excited states

6.2.1 Periodic calculations

For compounds **1**–**3**, the crystal structures were used as a starting point for subsequent calculations. For compound **4**, we used the crystal structure of a cyclohexyl-bridged derivative of our DADQs, obtained from an earlier publication[1] as a starting structure and manipulated the cyclohexyl unit by hand (Fig. S9). Periodic density

a = 9.4240(2)
b = 11.9409(2)
c = 12.0647(2)
α = 90
β = 91.446(2)
γ = 90

a = 7.88891
b = 11.40037
c = 12.15127
α = 89.9925
β = 87.5714
γ = 90.0418
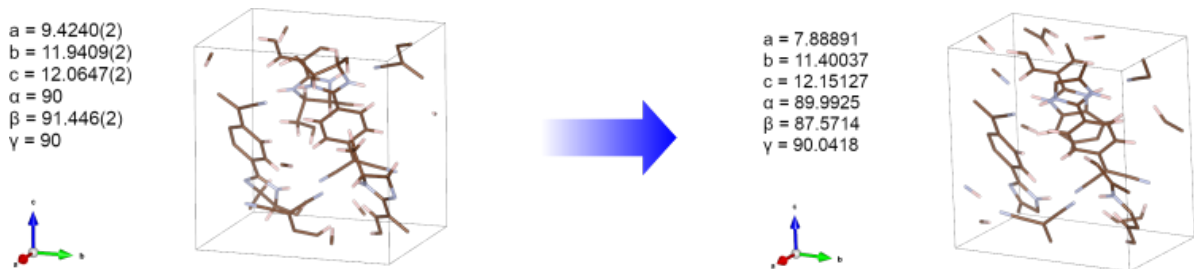
Figure S9: Unit cell and parameters of compound **4** after hand-manipulation of a the solid-state structure of a cyclohexyl-bridged DADQ derivative and subsequent solid-state optimisation (for details see down below).

functional theory (DFT) calculations at the PBE-D3(BJ)[5–7] level using VASP[8–10] were employed to optimise the solid state structures of compounds **1**, **2** and **4**. Plane-wave basis sets with an energy cutoff of 421 eV was used in combination with projector-augmented wave potentials.[11] The convergence threshold for the SCF cycles were set to 10^{-4} eV employing the blocked Davidson algorithm. Internal and external lattice parameters were relaxed using the conjugate-gradient algorithm with a force convergence parameter of 10^{-3} eV/Å^2 on a 6x6x6 k-grid constructed using the Monkhorst-Pack scheme.[12] For the bandstructure calculations, the k-grid was refined to 8x8x8 k-points and the energy cutoff was increased to 520 eV. For density-of-states (DOS) plots and partial charge densities (Figure 5 in main text), the k-grid was furthermore increased to 10x10x10. Partial charge densities were produced for the four lowest-lying unoccupied and four highest-lying occupied bands. Dielectric tensors were computed at the same energy cutoff on a 6x6x6 k-grid again. According to literature,[13] the eigenvalues of the dielectric tensor l_i can be used to calculate an effective static (zero frequency) dielectric constant,

$$\varepsilon = \frac{3 l_1 l_2 l_3}{l_1 l_2 + l_1 l_3 + l_2 l_3},$$

and the refractive index n is obtained as the square root of the average of the eigenvalues of the dielectric tensor,

$$n = \sqrt{(l_1 + l_2 + l_3)/3} \tag{1}$$

The obtained values for ε and n are summarised in **Table S7**. Furthermore, DOS plots were generated employing

Table S7: Dielectric tensor and refractive index obtained from periodic PBE calculations

	ε	n
1	3.247	1.823
2	3.582	1.946

the HSE06 functional[14] to compare to the PBE results (Figure 5 in main text). Due to the large unit cell sizes (224 atoms for **1**, 128 atoms for **2**), calculations were performed on a smaller 2x2x2 k-grid, the energy cutoff of 520 eV was however retained.
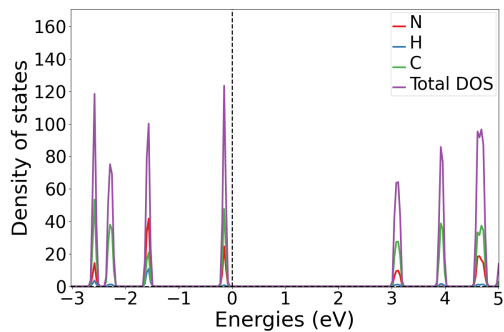
Figure S10: DOS plot of compound **1** obtained at the HSE06 level of DFT.
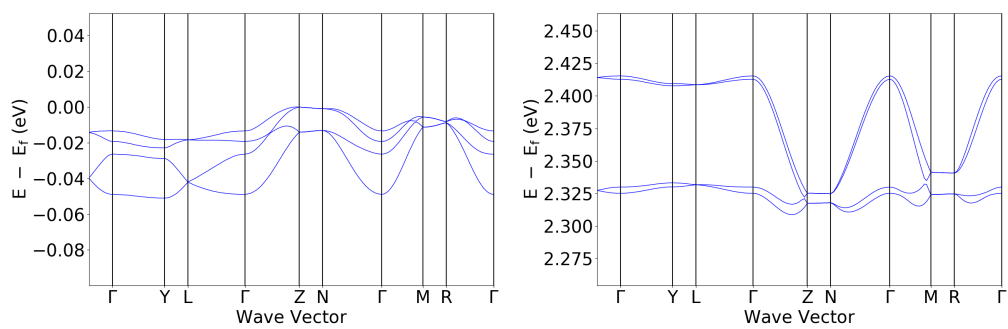
Figure S11: VB and CB of compound **1** obtained at the PBE level.
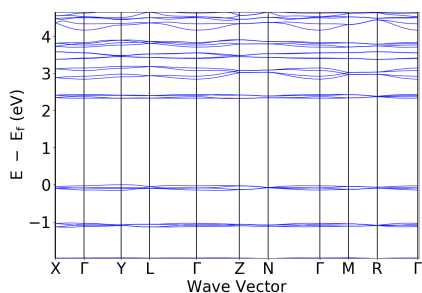
(a) Bandstructure of compound **2** obtained at the PBE level.
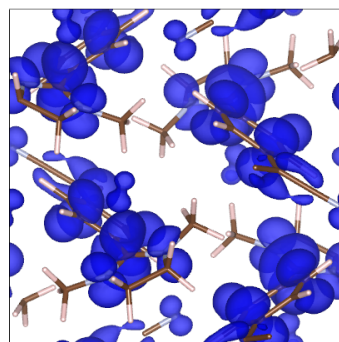
(b) LUMO charge density of compound **2** obtained at the PBE level, isovalue=$0.003a_0^{-3}$.
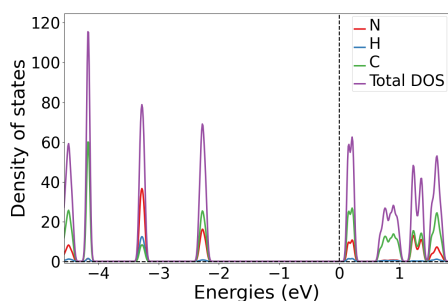
(c) DOS plot of compound **2** obtained at the PBE level.
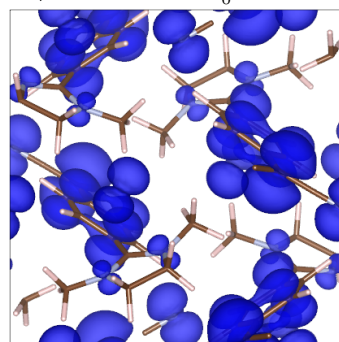
(d) HOMO charge density of compound **2** obtained at the PBE level, isovalue=$0.003a_0^{-3}$.
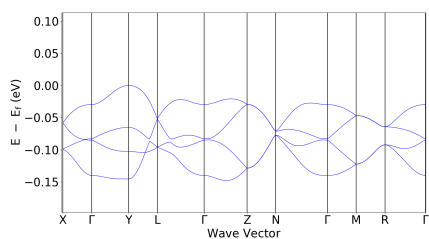
(e) VB of compound **2** obtained at the PBE level.
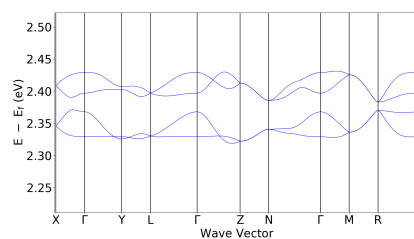
(f) CB of compound **2** obtained at the PBE level.
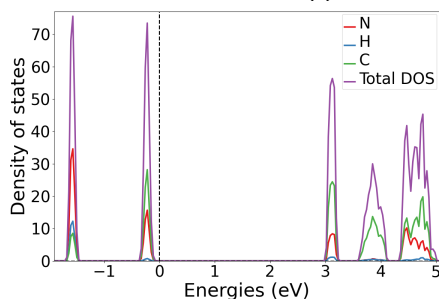
(g) DOS plot of compound **2** obtained at the HSE06 level.

Figure S12: Solid-state results for compound **2**.

6.2.2 TD-DFT calculations for oligomers

Time-dependent DFT (TD-DFT) calculations were performed at the ωB97X-D3/def2-SVP[3,4] level for various dimers, the unit cell tetramers, and an octamer of compounds **1** and **2** to estimate the locality of the electronic transitions in the solid state. For compound **2**, a dodecamer could also be calculated. As an approximation to the solid-state environment, the effective dielectric constant and refractive index obtained in the periodic calculations (**Table S7**) were used for the evaluation of the excited states. All structures are depicted in **Fig. S13** and **Fig. S14**. **Tables S7** to **S12** summarise all computed excited states with their transition energies and oscillator strengths. Figures S15 to S17 depict a selected few difference densities of the transitions with the highest oscillator strengths. Especially in the octamers and the dodecamer it can be observed that all transitions are fairly localised on either a monomer or a dimer with small contributions from anything else.
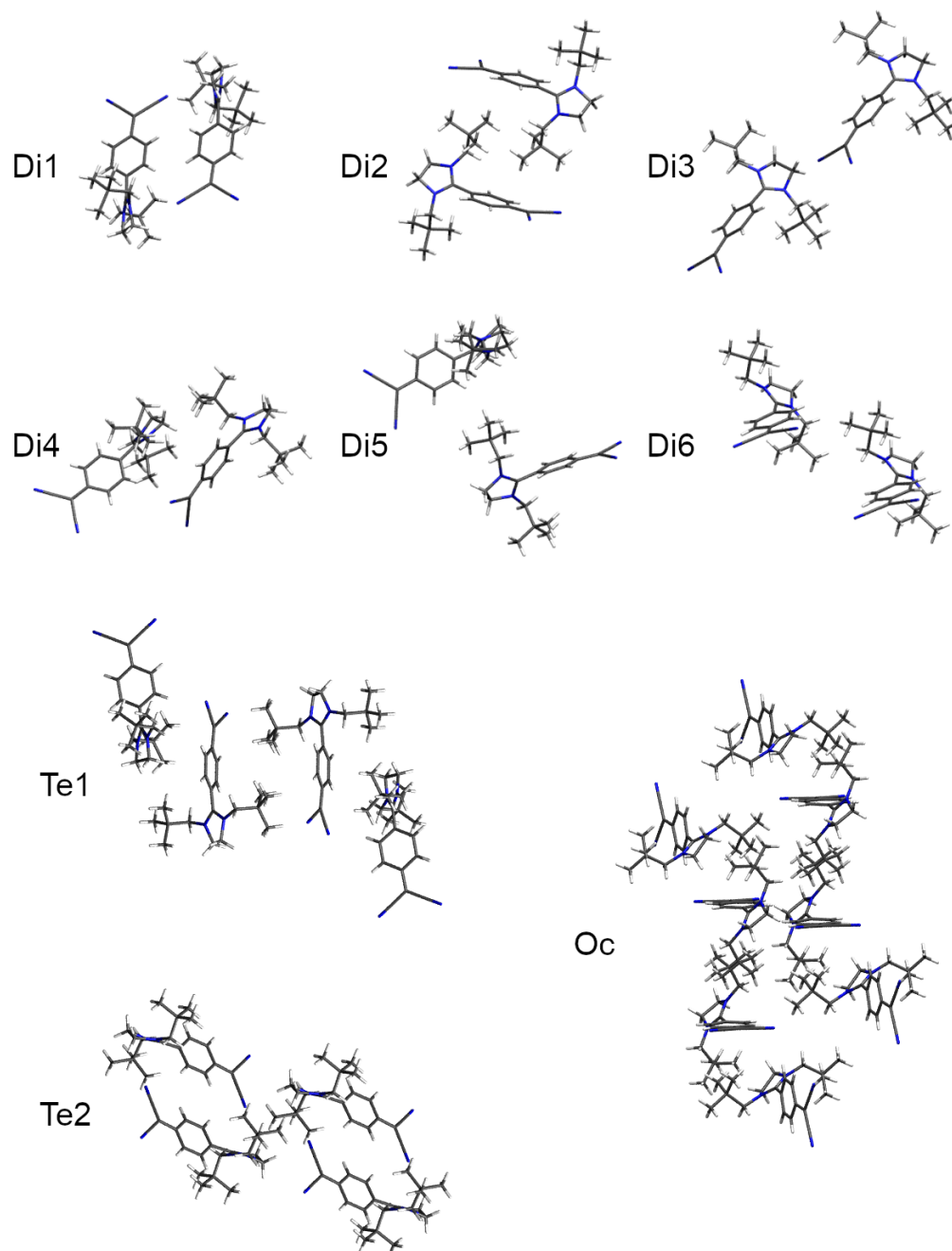
Figure S13: Oligomer structures of compound **1** used for TD-DFT evaluation.
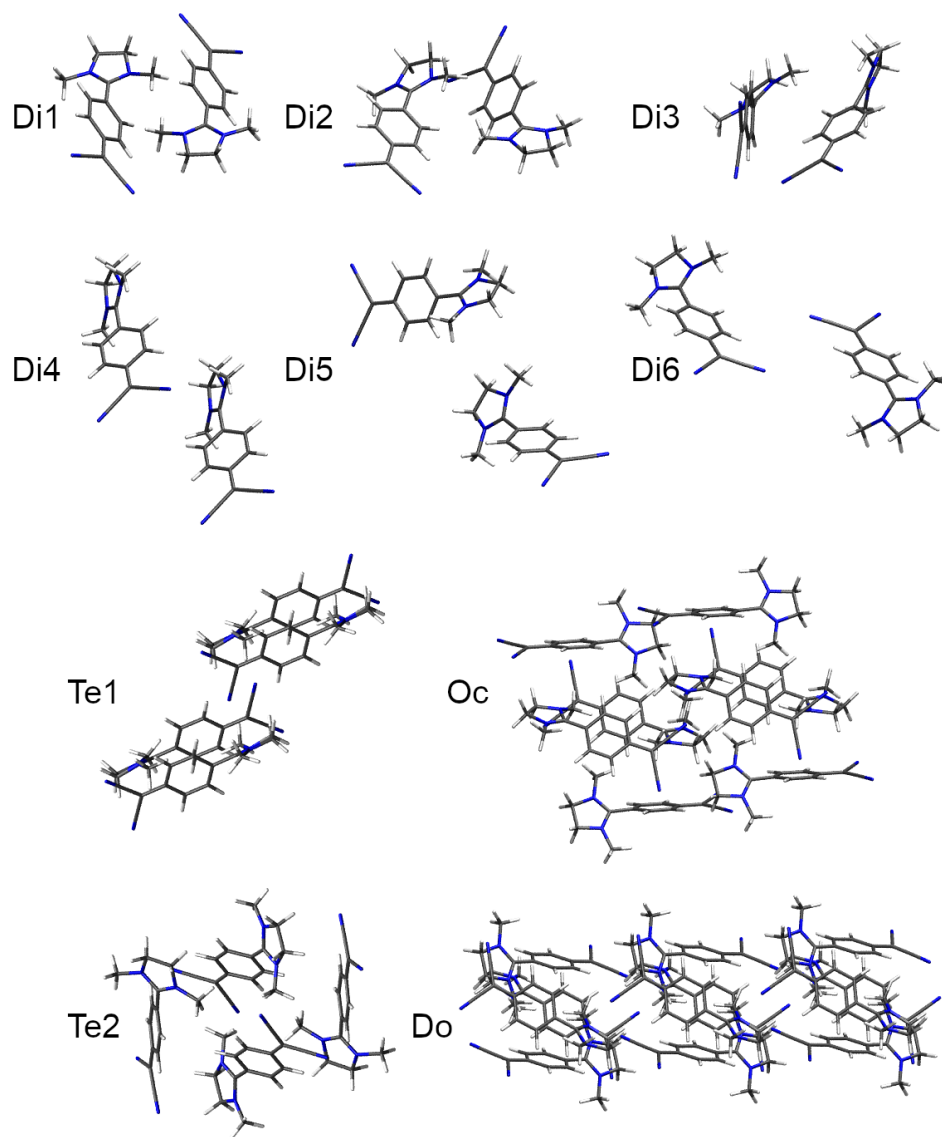
Figure S14: Oligomer structures of compound **2** used for excited-state calculations at the TD-DFT level.

Compound **1**:

Table S8: Excited state wavelengths in nm and oscillator strenghts of various dimers of compound **1** obtained at the ωB97X-D3/def2-SVP level of TD-DFT.

Structure	excited state	λ_{abs}	f_{osc}	Structure	excited state	λ_{abs}	f_{osc}
Di1	S_1	325.9	0.00	Di4	S_1	347.2	0.27
	S_2	312.5	1.16		S_2	346.1	1.02
Di2	S_1	332.7	0.00	Di5	S_1	335.8	0.02
	S_2	325.8	1.20		S_2	334.7	1.28
Di3	S_1	332.5	1.53	Di6	S_1	346.3	0.00
	S_2	325.6	0.02		S_2	341.2	1.24

Table S9: Excited state wavelengths in nm and oscillator strenghts of two tetramers of compound **1** obtained at the ωB97X-D3/def2-SVP level of TD-DFT.

Structure	excited state	λ_{abs}	f_{osc}	Structure	excited state	λ_{abs}	f_{osc}
Te1	S_1	332.9	0.00	Te2	S_1	321.5	0.00
	S_2	337.6	1.07		S_2	318.3	0.00
	S_3	334.3	0.00		S_3	310.7	2.81
	S_4	327.9	1.41		S_4	303.9	0.00

Table S10: Excited state wavelengths in nm and oscillator strenghts of an octamer of compound **1** obtained at the ωB97X-D3/def2-SVP level of TD-DFT.

Structure	excited state	λ_{abs}	f_{osc}
Oc	S_1	344.4	0.01
	S_2	344.3	0.00
	S_3	337.7	0.04
	S_4	338.0	0.00
	S_5	334.5	2.92
	S_6	334.8	0.02
	S_7	326.7	0.00
	S_8	314.0	1.40

Compound **2**:

Table S11: Excited state wavelengths in nm and oscillator strenghts of various dimers of compound **2** obtained at the ωB97X-D3/def2-SVP level of TD-DFT.

Structure	excited state	λ_{abs}	f_{osc}	Structure	excited state	λ_{abs}	f_{osc}
Di1	S_1	338.2	0.00	Di4	S_1	343.0	1.43
	S_2	325.4	1.27		S_2	335.1	0.10
Di2	S_1	340.2	0.14	Di5	S_1	350.5	1.37
	S_2	332.9	1.18		S_2	347.0	0.12
Di3	S_1	358.3	0.13	Di6	S_1	351.3	0.16
	S_2	351.3	1.15		S_2	350.9	1.27

Table S12: Excited state wavelengths in nm and oscillator strenghts of two tetramers of compound **2** obtained at the ωB97X-D3/def2-SVP level of TD-DFT.

Structure	excited state	λ_{abs}	f_{osc}	Structure	excited state	λ_{abs}	f_{osc}
Te1	S_1	339.5	0.00	Te2	S_1	332.2	0.00
	S_2	339.7	0.35		S_2	327.6	0.10
	S_3	339.6	0.00		S_3	320.9	2.66
	S_4	323.3	1.89		S_4	314.9	0.00

Table S13: Excited state wavelengths in nm and oscillator strenghts of an octamer and a dodecamer of compound **2** obtained at the ωB97X-D3/def2-SVP level of TD-DFT.

Structure	excited state	λ_{abs}	f_{osc}	Structure	excited state	λ_{abs}	f_{osc}
Oc	S_1	333.6	0.00	Do	S_1	320.7	0.00
	S_2	334.3	0.24		S_2	321.5	0.27
	S_3	332.7	0.00		S_3	318.0	0.00
	S_4	328.4	0.34		S_4	316.7	0.00
	S_5	328.3	0.18		S_5	317.2	0.53
	S_6	328.9	0.99		S_6	317.7	1.43
	S_7	317.3	3.12		S_7	311.8	0.54
	S_8	311.9	0.00		S_8	309.9	0.00
	—	—	—		S_9	308.0	0.00
	—	—	—		S_{10}	305.4	6.72
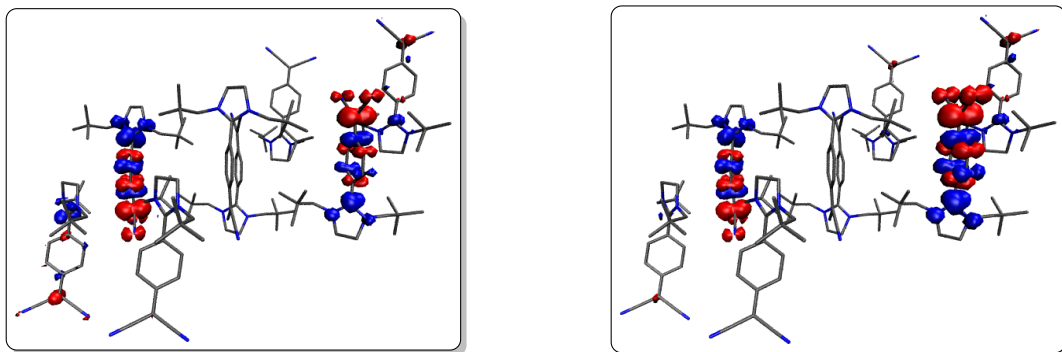
Figure S15: S_5 (left) and S_8 (right) difference densities of an octamer of compound **1**, isovalue = 0.001 a_0^{-3}. Blue and red zones correspond to areas of electron enhancement and electron depletion.
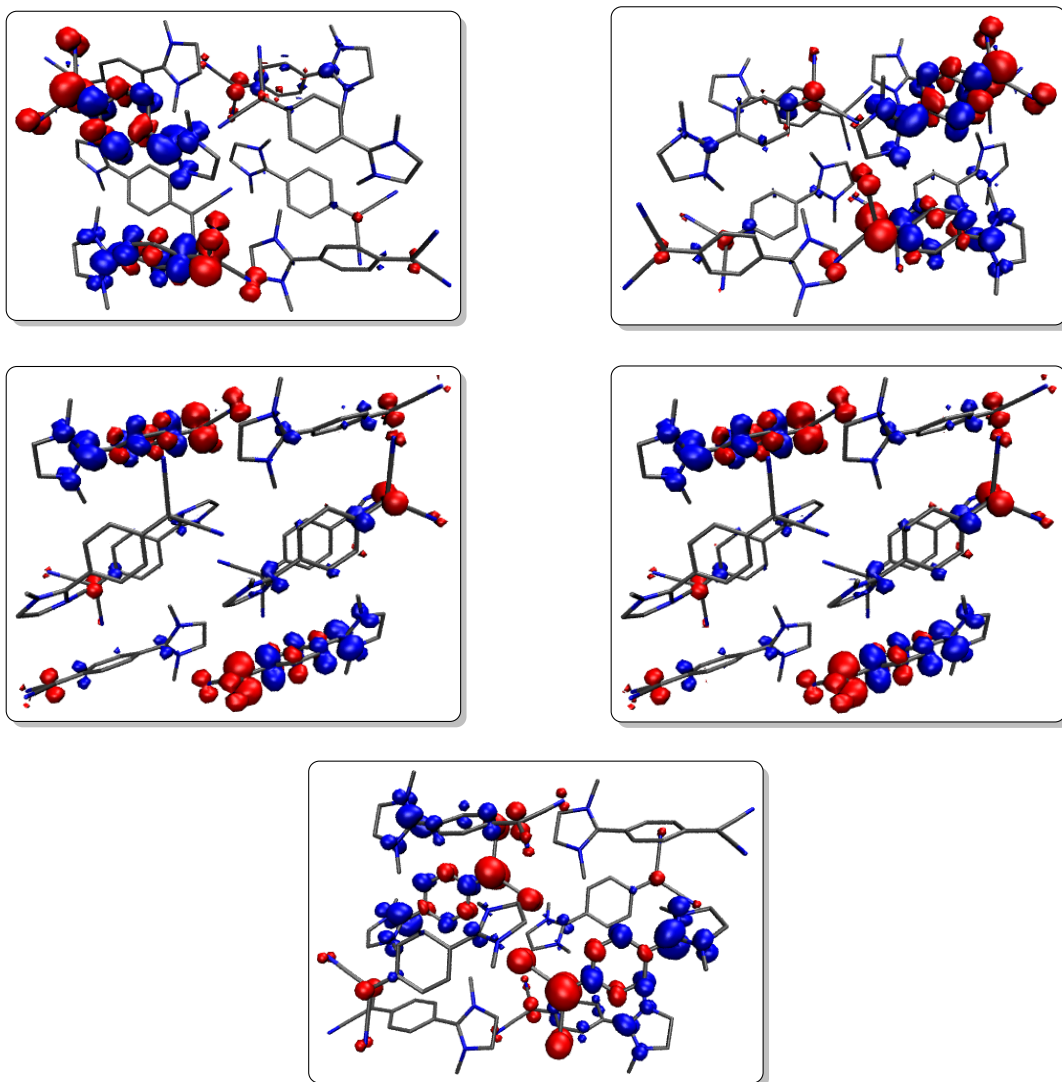
Figure S16: From top left to bottom right: S_2, S_4, S_5, S_6, and S_7 difference densities of an octamer of compound **2**, isovalue = 0.001 a_0^{-3}. Blue and red zones correspond to areas of electron enhancement and electron depletion. Note that the S_7 difference density is just comprised of two nodal structures localised on H-type dimers. However, it appears much more delocalised due to the inversion centre in the middle of the cluster which is somewhat difficult to discern in a static picture.
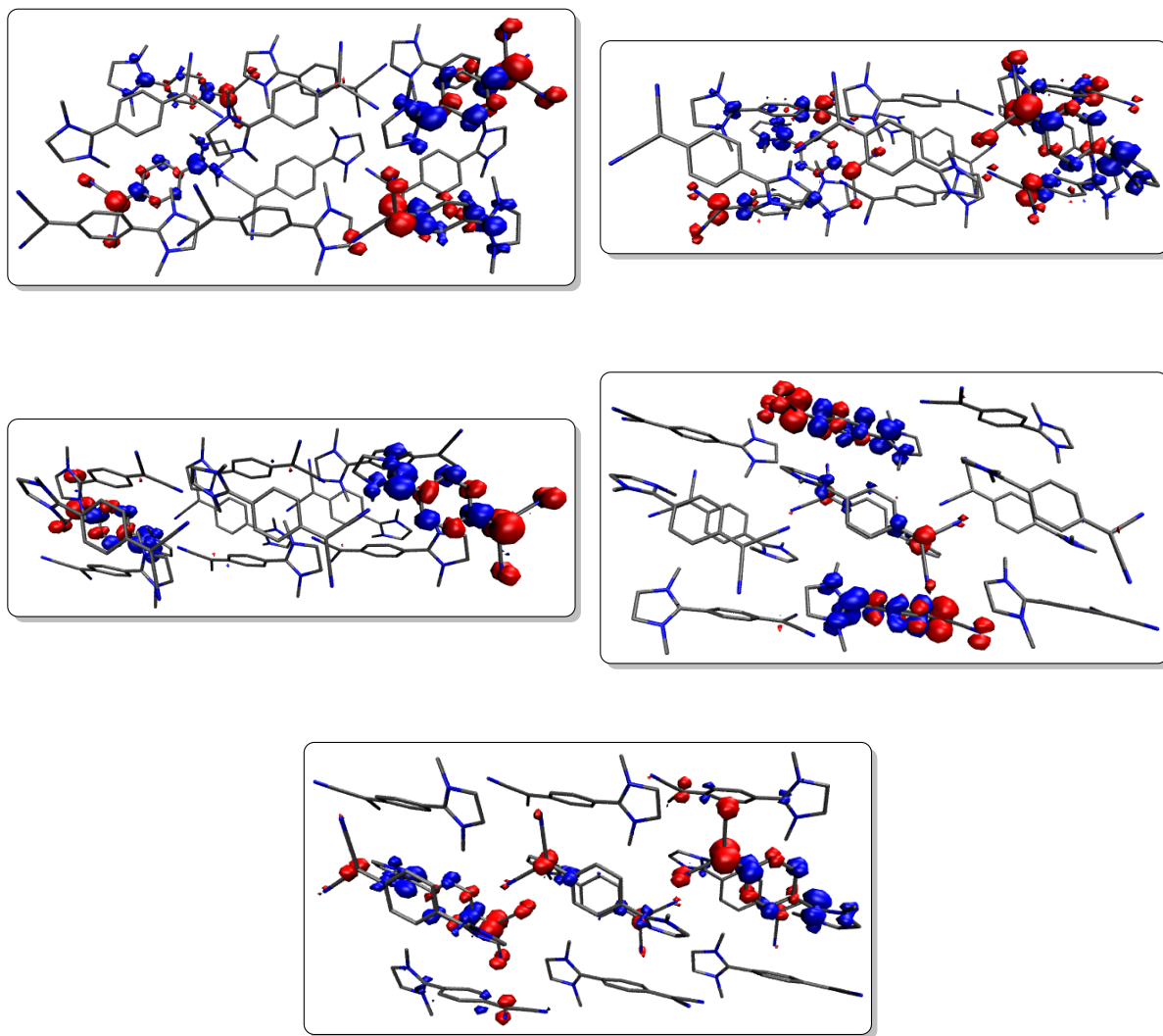
Figure S17: From top left to bottom right: S_2, S_4, S_5, S_6, and S_7 difference densities of an dodecamer of compound **2**, isovalue $= 0.001 \ a_0^{-3}$. Blue and red zones correspond to areas of electron enhancement and electron depletion.

6.2.3 QM/MM and DFT/MRCI calculations of monomers and dimers

In the next step, a 6x4x6 supercell of compound **1** and a 6x4x4 supercell of compound **2** (**Fig. S18**) were generated to mimic the crystal environment in a subsequent QM/MM optimisation of monomers and dimers (**Fig. S19**) embedded in their crystal structures. Gaussian's[15] ONIOM[16] scheme was utilised using the ωB97XD functional for the high layer and the universal force field (UFF) for the low layer. All atoms within 5 Å of the high layer atoms were allowed to relax during the run.
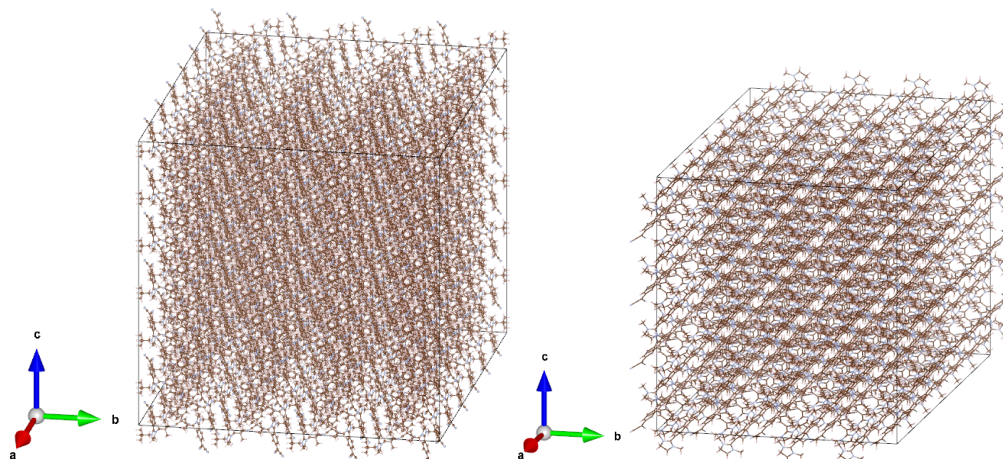
Figure S18: 6x4x6 supercell of compound **1** (left), 6x4x4 supercell of compound **2**.
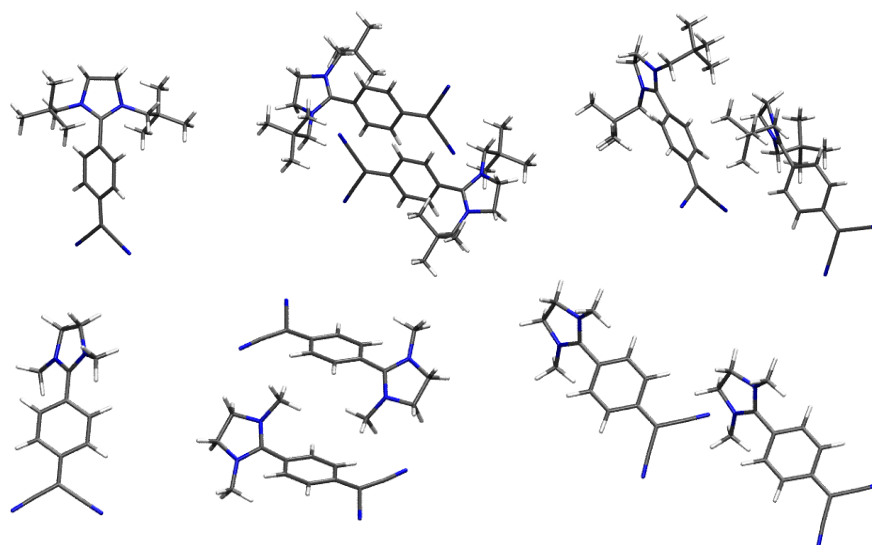
Figure S19: Structures examined in a QM/MM + DFT/MRCI study of compound **1** (top) and **2** (bottom).

First, a ground-state optimisation was performed succeeded by an excited-state optimisation of the state with the highest oscillator strength, which is the S_1 for monomers and J-aggregates, and the S_2 for H-aggregates. Afterwards, the trajectory of the excited-state optimisation is used to assess the PES of the bright state employing the DFT/MRCI[17–19] together with the C-PCM model[20] once again using the dielectric constant obtained from the periodic calculations. The minima of the S_0 and S_1 (or S_2 for H-dimers) then define the Stokes shift of the compounds and the emission peaks can be compared to experiment. **Table S14** summarises all excited states prior to and after optimisations with their transition energies and oscillator strengths. For the DFT/MRCI calculations, a reference space of 16 electrons and 14 orbitals with a default cut-off of 1.0 Hartree, which was carefully checked to not cut between degenerate orbitals, was chosen and all single and double excitations were incorporated. The reference space was refined once, i.e., two DFT/MRCI calculations were performed in succession. Initial testing found that a second refinement of the reference space did not yield any significant change in excitation energies or oscillator strengths.

Table S14: Absorption and emission wavelengths in nm, oscillator strengths, and lifetimes in ns of a monomer (mon), an H-type and a J-type dimer of compounds **1** and **2**

			λ_{abs} (calc.)	f_{osc} (abs)	λ_{em} (calc.)	λ_{em} (exp.)	f_{osc} (em)	τ (exp.)
1	mon	S_1	440	0.84	488	495	0.81	3.60 at 495 nm
	H-dimer	S_1	404	0.00	466		0.00	
		S_2	387	1.22	432	438*	1.38	0.86 at 435 nm
	J-dimer	S_1	444	0.87	507		0.82	
		S_2	430	0.77	439		0.75	
2	mon	S_1	412	0.81	463	463	0.73	1.35 at 460 nm
	H-dimer	S_1	409	0.00	439		0.00	
		S_2	392	1.35	419	— **	1.38	1.18 at 425 nm
	J-dimer	S_1	400	1.70	436		1.29	
		S_2	391	0.02	420		0.33	

* estimated from Gaussian fit, ** could not be estimated reliably

J-aggregate S_1 and S_2 difference densities (**Fig. S21**) are significantly localised on the monomer units, with the degree of localisation increasing during the excited-state optimisation. As a result, both the S_1 and the S_2 show non-negligible oscillator strengths especially for compound **1**. The usually smaller oscillator strength of the S_2 may be an alternative explanation for the high-energy shoulder encountered in the experimental emission spectra. However, for compound **2**, if we assume a large contribution from J-aggregates to the emission properties, we should expect a third intense band in between the main peak and the high-energy shoulder, which we do not observe, although this may be somewhat difficult to evaluate due to the dominating main emission peak. For compound **1**, we do see an agreement between experimental and calculated emission energies. However, J-type dimers should produce shorter lifetimes for the main peak due to the larger oscillator strength of the S_1. Furthermore, the localisation of the difference densities onto the monomer units indicates small intermolecular coupling in comparison to H-type dimers which show completey delocalised difference densities (**Fig. S20**). Due to the small intermolecular coupling and since they do not seem to significantly contribute to the emission properties, the term "J-aggregate" should in this context probably be taken with a grain of salt. In conclusion, J-type aggregation may play a minor hypothetical role, possibly for the spectral area in between main peak and high-energy shoulder and in polarising monomers. In general, however, monomers and H-aggregates determine the overall emission properties of DADQs in the solid state.
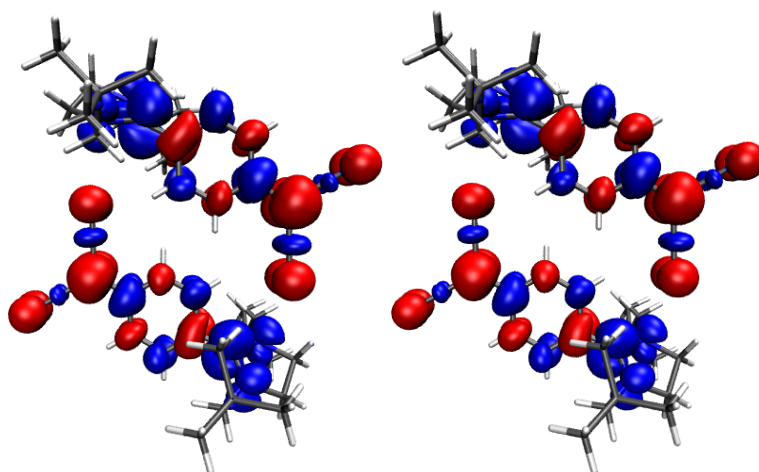
Figure S20: S_1 (left) and S_2 (right) difference densities of compound **1** in an H-type conformation, isovalue = 0.001 a_0^{-3}. Blue and red zones correspond to areas of electron enhancement and electron depletion.
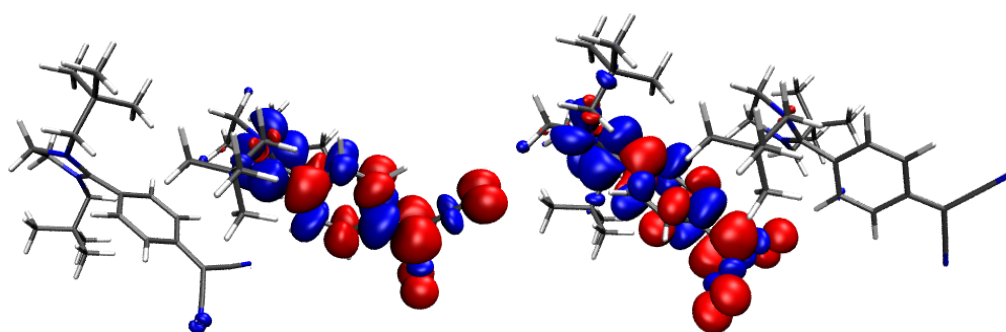
Figure S21: S_1 (left) and S_2 (right) difference densities of compound **1** in a J-type conformation, isovalue $= 0.001$ a_0^{-3}. Blue and red zones correspond to areas of electron enhancement and electron depletion.

7 Coordinates of molecular structures of all dimers

The cartesian coordinates of the monomers, H-dimers, and J-dimers of compounds **1** and **2** in ground and excited states will be provided in a separate file.

References

[1] P. Rietsch, F. Witte, S. Sobottka, G. Germer, A. Becker, A. Güttler, B. Sarkar, B. Paulus, U. Resch–Genger, S. Eigler, *Angew. Chem. Int. Ed.* **2019**, *58*, 8235–8239.

[2] P. Srujana, T. Gera, T. P. Radhakrishnan, *J. Mater. Chem. C* **2016**, *4*, 6510–6515.

[3] J.-D. Chai, M. Head-Gordon, *J. Chem. Phys.* **2008**, *128*, 084106.

[4] F. Weigend, R. Ahlrichs, *Phys. Chem. Chem. Phys.* **2005**, *7*, 3297.

[5] J. P. Perdew, K. Burke, M. Ernzerhof, *Phys. Rev. Lett.* **1996**, *77*, 3865–3868.

[6] S. Grimme, J. Antony, S. Ehrlich, H. Krieg, *J. Chem. Phys.* **2010**, *132*, 154104.

[7] S. Grimme, S. Ehrlich, L. Goerigk, *J. Comput. Chem.* **2011**, *32*, 1456–1465.

[8] G. Kresse, J. Hafner, *Phys. Rev. B* **1993**, *47*, 558–561.

[9] G. Kresse, J. Furthmüller, *Comput. Mater. Sci.* **1996**, *6*, 15–50.

[10] G. Kresse, J. Furthmüller, *Phys. Rev. B* **1996**, *54*, 11169–11186.

[11] P. E. Blöchl, *Phys. Rev. B* **1994**, *50*, 17953–17979.

[12] H. J. Monkhorst, J. D. Pack, *Phys. Rev. B* **1976**, *13*, 5188–5192.

[13] I. Petousis, W. Chen, G. Hautier, T. Graf, T. D. Schladt, K. A. Persson, F. B. Prinz, *Phys. Rev. B* **2016**, *93*, 115151.

[14] J. Heyd, G. E. Scuseria, M. Ernzerhof, *J. Chem. Phys.* **2003**, *118*, 8207–8215.

[15] M. J. Frisch, G. W. Trucks, H. B. Schlegel, G. E. Scuseria, M. A. Robb, J. R. Cheeseman, G. Scalmani, V. Barone, G. A. Petersson, H. Nakatsuji, X. Li, M. Caricato, A. V. Marenich, J. Bloino, B. G. Janesko, R. Gomperts, B. Mennucci, H. P. Hratchian, J. V. Ortiz, A. F. Izmaylov, J. L. Sonnenberg, D. Williams-Young, F. Ding, F. Lipparini, F. Egidi, J. Goings, B. Peng, A. Petrone, T. Henderson, D. Ranasinghe, V. G. Zakrzewski, J. Gao, N. Rega, G. Zheng, W. Liang, M. Hada, M. Ehara, K. Toyota, R. Fukuda, J. Hasegawa, M. Ishida, T. Nakajima, Y. Honda, O. Kitao, H. Nakai, T. Vreven, K. Throssell, J. Montgomery, J. A., J. E. Peralta, F. Ogliaro, M. J. Bearpark, J. J. Heyd, E. N. Brothers, K. N. Kudin, V. N. Staroverov, T. A. Keith, R. Kobayashi, J. Normand, K. Raghavachari, A. P. Rendell, J. C. Burant, S. S. Iyengar, J. Tomasi, M. Cossi, J. M. Millam, M. Klene, C. Adamo, R. Cammi, J. W. Ochterski, R. L. Martin, K. Morokuma, O. Farkas, J. B. Foresman, D. J. Fox, Gaussian16 Revision A.03, Wallingford, CT, **2016**.

[16] M. Svensson, S. Humbel, R. D. J. Froese, T. Matsubara, S. Sieber, K. Morokuma, *J. Phys. Chem.* **1996**, *100*, 19357–19363.

[17] C. M. Marian, A. Heil, M. Kleinschmidt, *WIREs Comput. Mol. Sci.* **2019**, *9:e1394*.

[18] I. Lyskov, M. Kleinschmidt, C. M. Marian, *J. Chem. Phys.* **2016**, *144*, 034104.

[19] M. Kleinschmidt, C. M. Marian, M. Waletzke, S. Grimme, *J. Chem. Phys.* **2009**, *130*, 044708.

[20] V. Barone, M. Cossi, *J. Phys. Chem. A* **1998**, *102*, 1995–2001.